NTNU – Trondheim
Norwegian University of
Science and Technology

Parallel Instabilities in Two-Phase Flow in Porous Media

Morten Vassvik

Physics
Submission date: May 2014
Supervisor: Alex Hansen, IFY

Norwegian University of Science and Technology
Department of Physics

Preface

The following thesis is submitted as part of the requirements for the Master's degree in physics, and concludes my studies at the Norwegian University of Science and Technology, (NTNU). It has been proposed by and written under the supervision of Professor Alex Hansen.

I have also been working in collaboration with guest researcher Santanu Sinha at NTNU, who helped me in writing the program used to perform simulations for this theses. His insight in the subject of network modelling and programming has been most valuable. I've also recieved invaluable guidance from Thomas Ramstad at Statoil ASA, whose own paper set the basis for the results presented in this thesis. Computational resources was allocated at the Department of Physics' UNIX cluster.

These last two semesters have been quite challenging, requiring a lot of hard work and ingenuity to arrive at where I am today. The time spent at the university has been most valuable to me, as I've learned a lot about programming and applied physics. Working on a problem as complicated as this one has taught me a lot on how to work by myself and in collaboration with others, and will be most useful in the future.

Trondheim, May 2014

Morten Vassvik

Acknowledgments

First, I would like to thank my supervisor Alex Hansen at NTNU for giving me the opportunity to work on such an interesting and unique subject as this. I would also like to thank Thomas Ramstad at Statoil for invaluable his knowledge and input, which has helped me greatly. I would also like to thank Santanu Sinha for helping me construct the program simulating the network model proposed in this thesis, as well as comments on this final manuscript. I would also like to thank Isha Savani, in addition to Alex Hansen and Santanu Sinha for providing interesting discussions and feedback during weekly meetings at NTNU. The assistance of Vegard Stenhjem Hagen should not go unnoticed. His help has been invaluable in the typesetting and proof-reading of this manuscript.

I would like to thank the lecturers and professors at NTNU who helped spark my interest in computational physics and programming, in particular Ingve Simonsen, Peter Berg, and Alex Hansen, which has lead me to where I am to this day.

And finally a big thank you goes for all the friends I've gotten to know during my stay in Trondheim, for making my stay a pleasant experience.

Abstract

Two immiscible fluids flowing in parallel with respect to the interface separating them in a two-dimensional porous medium has been studied using a dynamic network model. Two immiscible fluids, one wetting and the other non-wetting moving in parallel is a complicated process that haven't gotten much attention. It is found that there is a competition between imbibition and drainage displacements at the pore-scale along the front separating the two fluids due to an external force driving both the fluids in the direction parallel to this front. Imbibition is the process where a wetting fluid displaces a non-wetting fluid, while drainage is when a non-wetting fluid displaces a wetting fluid.

When an external force driving the system in the direction parallel to the front separating the two liquid is small, such that the capillary forces are much strong that viscous forces, we find that imbibition displacements will dominate along the front. The wetting fluid is found to displace the non-wetting such that the front separating the non-wetting fluid from the wetting fluid moves with a velocity proportional to the volumetric flow rate perpendicular to the imposed flow direction. A wetting fluid will prefer to displace a non-wetting fluid along narrow channels due to the fact that capillary forces provide suction in imbibition, as opposed to resistance in drainage. When the front is moving, we find that clusters of non-wetting fluids are left behind the front, concentrated in the widest part of the network. These cluster will not be able to be move as long as the external driving force is not large enough to overcome the the capillary forces holding back the cluster. Wetting fluid will flow in the space around the clusters.

If the external driving force is large enough so that these clusters can be mobilized, then we'll have viscous forces start dominating, and there will be a mixture of imbibition and drainage depending on the local geometry and boundary conditions. If drainage starts dominating the front will stop moving and become unstable, and non-wetting fingers will start moving in the direction of the wetting liquid. If the driving force is strong enough, these fingers will break up into bubbles due to crossing wetting fluids, and non-wetting bubbles will start migrating into the wetting fluid.

For special case of a band of non-wetting fluid surrounded by wetting fluid on both sides, we find that the wetting fluid will try to displace the non-wetting fluid from both sides simultaneously. If the external driving force is not strong enough so that the clusters broken off from either side can be mobilized, we find that both the fronts stabilize and stop moving. The non-wetting and wetting fluid will then flow by themselves as if they were part of its own effective network separated by the fluid-fluid front, without any influence from the other fluid. The two fronts will be stationary as long as the capillary forces are dominating over viscous forces.

Sammendrag

To ikke-blandbare væsker som strømmer parallelt i forhold til hverandre i et todimensjonalt porøst medium har blitt utforsket ved hjelp av en dynamisk nettverksmodell. To ikke-blandbare væsker, én fuktende og en ikke-fuktende som beveger seg parallelt med grensesjiktet som skiller de to væskene viser seg å være en komplisert prosess. Det viser seg at det vil oppstå en konkurranse mellom imbibering (Engelsk: imbibition) og drenering (Engelsk: drainage) lokalt langs fronten som skiller de to væskene. Imbibering er når en fuktende væske forflytter en ikke-fuktende væske, mens drenering er når en ikke-fuktende væske forflytter en fuktende væske,

Når den eksterne kraften som driver systemet i retningen parallelt med grensen mellom de to væskene er liten, slik at kapillærkrefter er sterkere enn viskøse krefter, så viser det seg at imbibering dominerer langs fronten. Den fuktende væsken forflytter den ikke-fuktende væsken slik at fronten som skiller de to væskene gradvis beveger seg mot den ikke-fuktende væsken med en hastighet som er proporsjonal med volumstrømningen på tvers av den parallele retningen. En fuktende væske vil foretrekke å forflytte en ikke-fuktende væske langs smale kanaler siden kapillærkrefter gjør det enklere for en væske å flyte under imbibering. Når fronten forflyttes så vil klynger av ikke-fuktende væsker bli etterlatt bak fronten, konsentrert i de største kanalene. Dersom drivkraften som driver systemet ikke er stor nok til at kapillærkreftene som holder igjen disse klyngene kan overkommes, så vil de sitte fast, mens fuktende væske flyter i rommet rundt de.

Dersom kraften som driver systemet blir sterk nok til at klyngene med ikke-fuktende væske kan mobiliseres, så vil viskøse krefter starte å dominere, og det vil forekomme en blanding av imbibering og drenering. Hvilken av disse som dominerer avhenger av den lokale geometrien, og på grensebetingelsene i det porøse mediet. Dersom drenering dominerer, så vil fronten slutte å forflytte seg mot den ikke-fuktende væsken og bli ustabil, og ikke-fuktende fingrer vil vokse inn i den fuktende væsken. Dersom drivkraften er sterk nok, så vil disse fingrene brytes opp på grunn av passerende fuktende væsker, og ikke-fuktende bobler vil migrere ut i den fuktende væsken.

Dersom et bånd av ikke-fuktende væske er omringet av fuktende væske på begge sidene, så vil den fuktende væsken prøve å forflytte den ikke-fuktende væsken fra begge sidene samtidig. Dersom den eksterne drivkraften ikke er kraftig nok til at klyngene med ikke-fuktende bobler som oppstår bak frontene kan forflyttes, så vil frontene stoppe opp, og den ikke-fuktende og den fuktende væsken vil flyte hver for seg i hver sitt effektive nettverk, uten påvirkning av den andre væsken. Disse frontene vil forbli stasjonære så lenge kapillærkrefter dominerer over viskøse krefter.

Contents

1. Introduction

Multiphase flow in porous media spans a wide portion of applied physics and industries, from cosmetics, to agriculture, and oil recovery. Understanding how multiple fluids interact in a porous material is integral in areas such as improved and enhanced oil recovery in the petroleum industry. Perhaps just as important in modern times is its application to underground water extraction in water-starved areas.

The flow of immiscible fluids in porous media is a phenomenon governed by physics at multiple scales. On the macroscopic scale the flow is described by phenomenological and theoretical continuum differential equations relating macroscopic quantities such as total flow rate, fluid saturation, fractional flow, permeabilities and pressure. Examples of these are continuum equations such as the Buckley-Leverett [1] and the Darcy equation [2]. The solution to these equations represent averages over representative volumes, and we often need to neglect or simplify the effect at the pore-scale, phenomenon such as capillary pressures. Experiments are usually done in the lab by taking a small sample of a porous material, from which the relevant macroscopic quantities such as the permeability is calculated. These are then assumed to apply for the larger scales.

Computer simulations based on the physics at the pore scale has become more popular during the last few decades, providing an alternative to performing time consuming, expensive laboratory experiments. Not only are they often cheaper and much faster to perform, but they have also become able quantitatively estimate and predict the macroscopic properties of interest in a real porous medium.

Lab experiments and computer simulations of the flow at the pore scale have mostly focused on the displacement of one fluid by another by injecting one fluid into a sample already filled by another liquid, and a huge effort has gone into classifying and understanding how the behavior of the displacement processes depend on the flow properties such as viscosity ratios and wetting properties. Not much focus has yet been given to the case where two immiscible fluids are flowing in parallel to the interface separating the two fluids inside a porous medium. A real life application of this could be the study of stratified reservoirs, where different phases are deposited in layers. One could also imagine the case of a non-wetting fluid inhabiting a large part of a reservoir, with a wetting fluid surrounding it. The study of parallel flow would then concern itself with the flow along the sides of the non-wetting fluid.

1.1. Outline

This thesis is outlined as follows. Chapter 2 gives an introduction to the microscopic physics of two-phase flow at the pore-scale, and introduce the concept of parallel flow. Chapter 3 describes the simulation model in detail. Chapter 4 discusses the results found from implementing the simulation model. Concluding remarks are given in Chapter 5.

2. Flow in Porous Media

On the microscopic pore scale the multiphase flow is governed by the competition of viscous forces in the fluids, capillary forces due to local interfaces separating the fluids called menisci, and gravitational forces. These are described by the fundamental equations of fluid mechanics.[1] These equations can in principle only be solved for the simplest geometries and a limited range of parameters, such as Stokes flow[2] in a cylindrical channel.

The main focus of this thesis will be on microscopic physics on the pore scale. The relations and equations governing macroscopic flow in reservoirs will therefore not be covered. The reader should refer to Bear [3] and Sahimi [4] for a comprehensive review of macroscopic multiphase flow in porous media.

2.1. Microscopic Physics

2.1.1. Interfacial Tension

Assuming that the temperature is constant, then a static spherical droplet of radius R immersed in another fluid (e.g. a gas bubble in water) will have a surface free energy of $4\pi R^2\gamma$, where γ is the surface tension, representing the free energy per surface area. If the radius of the spherical droplet is changed by $\mathrm{d}R$, the corresponding change in surface free energy is $8\pi R\gamma\,\mathrm{d}R$. This change in energy must be balanced by the pressure between the inside of the droplet and its surroundings, $\Delta p \cdot 4\pi R^2\,\mathrm{d}R = 8\pi R\gamma\,\mathrm{d}R$. Solving for Δp gives

$$\Delta p = \frac{2\gamma}{R}. \tag{2.1}$$

Equation (2.1) can alternatively be derived from hydrodynamical considerations. The surface free energy is due to the difference between the attraction of the molecules on the inside of the sphere (water), those outside of the sphere (air), and those at the surface between the two fluids.

The general form of (2.1) is known as the Young-Laplace equation

$$\Delta p = \gamma\left(\frac{1}{R_1} + \frac{1}{R_2}\right), \tag{2.2}$$

[1] E.g. The Navier-Stokes equations.

[2] Stokes flow, also known as *creeping motion*, is when viscous forces dominate over inertial forces, which is to say that the Reynolds number is much less than unity, e.g. $\mathrm{Re} = \mu UL/\rho \ll 1$, where U and L are relevant velocity and length scales in the problem at hand. μ and ρ is the viscosity and density of the fluid in question, respectively.

where R_1 and R_2 are the principal radii of curvature of the general surface. For a perfect sphere they reduce to the same radius of curvature. Equation (2.2) assumes a surface in thermodynamical and hydrodynamical equilibrium. It will not hold in general if either the surface is moving, or if the temperature is not constant.

2.1.2. Wettability

The wettability is defined as the contact angle, θ between the surface separating two immiscible fluids in thermal equilibrium on a horizontal solid surface, as depicted in Figure 2.1. The wettability is a thermodynamic quantity that depends on the interfacial tensions of the liquid-gas or liquid-liquid surfaces as well as the interactions between the liquids and the material of the solid surface. A fluid is wetting the solid surface if $90° < \theta < 180°$, and non-wetting if $0° < \theta < 90°$. $\theta = 0°$ and $\theta = 180°$ is called completely non-wetting and wetting, respectively.

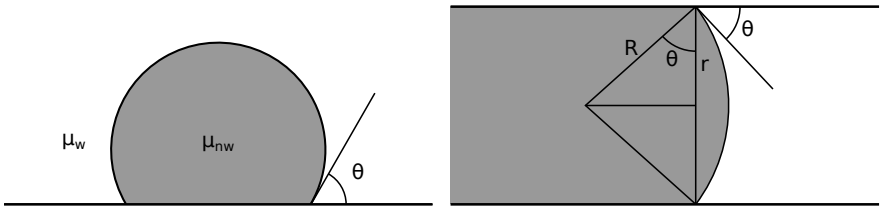

(a) (b)

Figure 2.1.: **(a)** Definition of contact angle by the interface separating the two fluid phases in contact with a solid surface. **(b)** A meniscus separating a non-wetting (gray) and a wetting (white) fluid inside a tube. The radius of curvature of the surface is given as $R = r/\cos\theta$, where θ is the contact angle.

The pressure difference across a stationary meniscus separating two fluid phases in a straight cylindrical tube of radius r is according to Figure 2.1b given by

$$p_c = \frac{2\gamma}{r}\cos\theta. \tag{2.3}$$

p_c is called *the capillary pressure*. If the meniscus is moving the contact angle will depend on the local flow rate in the tube, and whether it is receding or advancing [6].

2.2. Displacements in Porous media

Lenormand studied the large scale 2D displacement of immiscible fluids in micro-channels where gravitational forces could be neglected both experimentally [7], and numerically [8]. The experiments where done by injecting a fluid (the invading fluid) into a porous matrix already filled by another fluid (the defending fluid), displacing it in the process. He showed that in certain limits that the flow regimes

could be described by statistical models such as invasion percolation, and diffusion limited aggregation.

There are two main displacement categories, imbibition and drainage. Drainage is the process where a non-wetting fluid (with respect to the porous medium) displaces a wetting fluid. In drainage the fluid in the larger throats will be displaced first because of capillary effects due to menisci separating the non-wetting and wetting fluids gives resistance to motion. Drainage is dominated by piston-like displacements [7].

Imbibition is the process where a wetting fluid displaces a non-wetting fluid. Non-wetting fluids can only flow in the bulk of the pores and throats in the porous media, while the wetting fluid can either flow in the bulk, or along the walls and crevices of the throats (film flow). Imbibition is governed by the competition between piston-like motion and snap-off of the non-wetting phase due to wetting films [7, 9] flowing along the walls and crevices of the porous matrix. We therefore need to distinguish between the cases where film flow dominates, and where it can be neglected.

The capillary number describes the ratio of viscous to capillary forces on the pore scale. Its definition is

$$Ca = \frac{\mu_i u_i}{\gamma}, \tag{2.4}$$

where μ_i is the viscosity of the invading fluid, u_i is the mean velocity, and γ is the interfacial tension due to the menisci separating the two fluids. The viscosity ratio between the invading and defending fluids is

$$M = \frac{\mu_i}{\mu_d}. \tag{2.5}$$

These two non-dimensional number together characterize the displacement processes.

2.2.1. Drainage

There are three main distinct flow regimes for drainage, depending on the capillary number and viscosity ratio. The three main flow regimes are capillary fingering, viscous fingering, and stable displacement [8].

When a more viscous fluid displaces a less viscous fluid at high capillary numbers the displacement front is unstable and shows viscous fingering, where fingers of non-wetting fluid displace the wetting fluid. The front growth in viscous fingering can be statistically modelled by Diffusion-Limited Aggregation (DLA), and has a well defined fractal dimension. When a less viscous fluid displaces a more viscous fluid at high capillary numbers, the displacement process is called stable displacement, and is modelled by Anti-DLA. At low capillary numbers the capillary forces will dominate over viscous forces in both the fluids. The pressure is just large enough so that only some throats and pores can be invaded, giving rise to capillary fingering. This regime is modelled by invasion percolation.

2.2.2. Imbibition

The flow regimes in imbibition are controlled by the competition between piston-like motion and snap-off during pore scale displacements. For low capillary numbers and small contact angles the displacement is governed by snap-off, where the wetting phase flows along the walls and crevices of the porous medium. This resembles a percolation-like regime, where snap-off happens randomly across the entire system due to the connectedness between the wetting films along the walls. If the contact angle or capillary number is increased, the snap-off ahead of the front will be suppressed due to there not being enough time for the wetting fluid to flow along the walls. This is because the piston-like behavior depend on the local capillary number, while the snap-off is a diffusive process independent of the capillary number. For large capillary numbers the displacements in imbibition are similar to a large Ca displacements in drainage [7].

2.2.3. Parallel Flow

Drainage and imbibition are processes of displacing one fluid by another fluid. These terms are usually used to describe the displacement process when the front separating the two fluids grow in the direction of the applied driving force, e.g. it the force is applied perpendicular to the front. If the front separating the two fluids is parallel to direction of the driving force one would expect both drainage and imbibition locally along the front.

The study of parallel flow has gotten little attention in the litterature until now. Ramstad *et al.* [10] used a dynamical network simulator to study parallel flow. A two-dimensional porous media was modelled as a square grid of disordered tubes rotated 45 degrees. He investigated the case of a network initially filled by a band of non-wetting fluid surrounded on both sides by a wetting fluid where both sides of the network are connected to an open reservoir of wetting fluid. The flow was driven by a constant pressure gradient in the direction parallel to the fronts separating the two phases. It was found that the front separating the band of non-wetting fluid from the wetting fluid became unstable when the pressure difference across the system reached a critical value, for which the fronts started moving towards the non-wetting liquid with a constant velocity and with a well-defined saturation profile, and with no wetting fluid moving ahead of the front. Behind the front there was a foam-like wake of non-wetting bubbles diffusing away from the front and eventually exiting the system through the open boundaries.

The opposite case of a wetting band surrounded by a non-wetting fluid connected to non-wetting reservoirs were also studied. In this case it was found that the fronts eventually stabilized and did not move, due to the wetting fluid not being able to move out of the system, and the transport of bubbles of non-wetting bubbles in each direction cancelled.

2.3. Flow in Tubes

2.3.1. Single Phase Flow - The Hagen-Poisuelle Equation

The volumetric flow rate of a single phase flowing through a tube of constant cross-section is given by the Hagen-Poiseuille equation. Its derivation can be found in any introductory fluid mechanics book, e.g. [11]. It can be expressed as

$$q = -\frac{kA}{\mu}\frac{\mathrm{d}p}{\mathrm{d}x} = -\frac{kA}{\mu L}\Delta p \tag{2.6}$$

This equation holds for a tube of arbitrary shape of constant cross-section A. For a cylindrical tube of radius r, and no-slip at the tube wall, we will have $k = \frac{r^2}{8}$, and $A = \pi r^2$.

The Hagen-Poiseuille equation is equivalent to Ohm's law for electrical circuits, with voltage and current being equivalent to pressure and flow rate, respectively.

2.3.2. Two-Phase Flow - The Washburn Equation

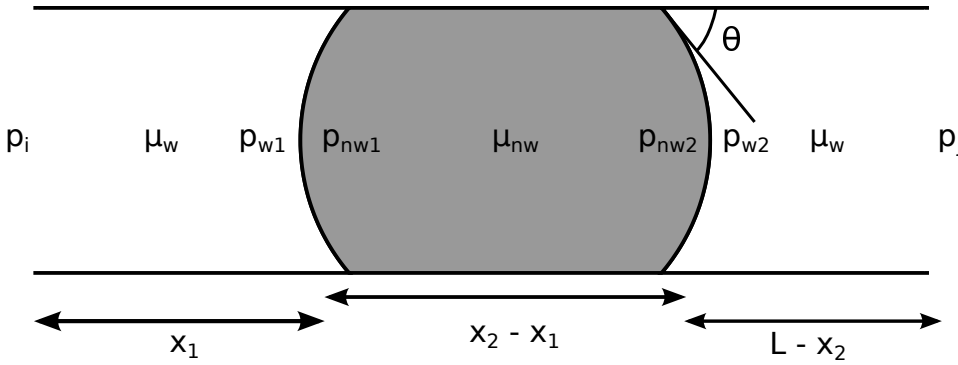

Figure 2.2.: Illustration showing the different pressures inside a cylindrical tube containing a single non-wetting bubble.

If a tube is filled with two immiscible fluids, one wetting with respect to the tube wall, and one non-wetting, then the flow rate in each phase satisfies equation (2.6) individually, and the flow rate is the same in each phase. The two phases will be separated by a meniscus, which means there will be a higher pressure on the inside of the meniscus due to interfacial tension along the surface. This results in a pressure jump across the meniscus.

With respect to figure 2.2, where we have a bubble of non-wetting fluid surrounded by a wetting fluid inside a straight circular tube of constant radius, we have for each phase separately

$$q = -\frac{kA}{\mu_w x_1}\Delta p_{w1} = -\frac{kA}{\mu_{nw}(x_2 - x_1)}\Delta p_{nw} = -\frac{kA}{\mu_w(L - x_2)}\Delta p_{w2}, \tag{2.7}$$

where the pressure differences are defined as

$$\Delta p_{w1} = p_{w1} - p_i, \tag{2.8}$$
$$\Delta p_{nw} = p_{nw2} - p_{nw1}, \tag{2.9}$$
$$\Delta p_{w2} = p_j - p_{w2}. \tag{2.10}$$

In addition, we define the total pressure difference, and the capillary pressures as

$$\Delta p_{c1} = p_{nw1} - p_{w1}, \tag{2.11}$$
$$\Delta p_{c2} = p_{w2} - p_{nw2}, \tag{2.12}$$
$$\Delta p = p_j - p_i. \tag{2.13}$$

Explicitly writing out the total pressure difference gives

$$\Delta p = (p_{w1} - p_i) + (p_{nw1} - p_{w1}) + (p_{nw2} - p_{nw1}) + (p_{w2} - p_{nw2}) + (p_j - p_{w2}). \tag{2.14}$$

After using equation (2.7), solving for q yields

$$q = -\frac{kA}{\mu_{eff} L}(\Delta p - p_{c1} - p_{c2}). \tag{2.15}$$

Equation (2.15) is called the Washburn equation, named after Washburn, who studied the the model with air displacing water [5]. A positive flow rate corresponds to a negative net pressure difference $\Delta p - \sum p_{ci}$, hence the minus sign. The effective, volume weighted viscosity is

$$\mu_{eff} = \mu_{nw} \frac{x_2 - x_1}{L} + \mu_w \frac{L - (x_2 - x_1)}{L}. \tag{2.16}$$

The average velocity through the tube will be given by

$$u = \frac{q}{A} = -\frac{k}{\mu_{\text{eff}} L}(\Delta p - p_{c1} - p_{c2}). \tag{2.17}$$

No restrictions has been made for the functional form of the capillary pressure. If the flow rate is small, then we are close to hydrodynamic equilibrium. The capillary pressure is then given by the Young-Laplace equation. For a straight capillary tube, the contact angle will then be the same on each side of a bubble, and the net capillary pressure will vanish. For larger flow rates experiments have shown that the receding and advancing contact angle will be different, with the receding contact angle being the largest. This is called a dynamic contact angle, and depend on the local capillary number in the tube [6].

We assume that there are no films. This is a valid assumption when using cylindrical shaped tube, which has no corner or crevices for films to flow through.

2.4. Network Simulators

All fluid behavior is governed by the fundamental equations of fluid mechanics and constitutive relations. These are solvable for only a very small subset of problems due to complex boundary conditions and non-linearities in the equations. The fluid mechanical equations can be solved numerically by methods such as finite elements, finite volume, or Lattice Boltzmann methods, but these are still only solvable for relatively small systems and simple geometries, and will not in general be able to give useful results on larger scales. An alternative approach termed network simulators has become popular during the last decades.

Network simulators exchanges solving the equations of fluid mechanics explicitly by replacing the complex geometry by a simplified network of connected volumes. In each of these volumes an analytical result is used to approximate the flow through it. An example of this would be a network of spherical volumes connected by cylindrical tubes representing pores and throats of a porous medium, respectively, or having the tubes representing both the pore and throat volume. Simple analytical solutions such as (2.6) are then applied as an approximation to the flow in each volume. Conservation of mass and flow rate are applied to solve for the local flow behavior, after which the state of each volume can be updated according to the local, instantaneous flow rates.

The first network model was proposed by Wilkinson and Willemsen to study invasion percolation [12]. Later Lenormand *et al.* used a more sofisticated network model to model both drainage and imbibition [8]. Other models such as the one developed by Aker *et al.* [13] allows menisci to have a position dependent capillary pressure, as opposed to the more simple constant capillary pressures of the model of Lenormand et al.

3. The Simulation Model

3.1. Description of the Model

3.1.1. Geometry

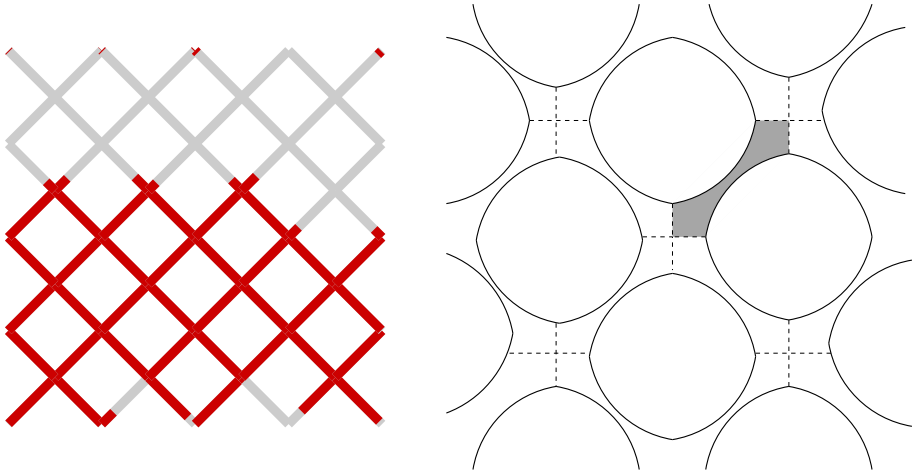

(a) (b)

Figure 3.1.: **a)** Visualization of non-wetting (red) and wetting (gray) fluids in a network of 8x8 links. **b)** Mapping of the network model to a porous medium consisting of the space between spherical shaped beads. The tubes, one marked in gray, corresponds to the links in the network, while the intersection of the dashed lines corresponds to the nodes.

The simulation model used is a dynamic network model based on a model previously developed by Aker *et al.* [13], with later extensions by Knudsen *et al.* [14], Ramstad *et al.* [15] and Sinha *et al.* [16]. The model geometry is a 2-dimensional regular square lattice of cylindrical tubes of random radii rotated 45 degrees. The bonds (links) of the grid contain to both the pores and throat volume of a 2-dimensional porous medium, that is, the nodes contain no volume, but has only a pressure associated with it. The grid is disordered, in the sense that each tube has a random radius uniformly distributed on the interval $[\lambda_1 L, \lambda_2 L]$, where $0 < \lambda_1 < \lambda_2 < 1$ and L is the length of the tube. Refer to Figure 3.1 for an illustration.

3.1.2. Flow Conditions

The system contains two fluids, one non-wetting (e.g. oil), and one wetting (e.g. water) with respect with the walls of the network. It is assumed that both fluids are incompressible and immiscible, which leads to a well defined interface, a meniscus, separating the two fluids. There will be a pressure jump across the meniscus due to its curvature, with the pressure being higher inside the curved surface. The strength of this capillary pressure is given by the surface tension γ. It is assumed that the contact angle is larger than zero, and that there are no wetting films present. The contribution of the contact angle to the capillary pressure is contracted into the surface tension coefficient itself.

The network is periodic with respect to pressure in all directions, but is open with respect to fluid flow on the sides, e.g. the sides are connected to a reservoir. It is periodic with respect to pressure in the vertical direction.

A global pressure difference across the system drives the flow in the y-direction. The pressure is calculated at all the nodes, and the local flow rates and velocities are found, from which the system is evolved for a single time step and the process is repeated.

3.1.3. Flow in a Single Tube

The flow rate through link ij connecting node i and j, containing two fluids, is governed by the Washburn equation:

$$q_{ij} = -\frac{A_{ij}k_{ij}}{\mu_{\text{eff}}L}\left(\Delta p_{ij} - p_{c,ij}\right) \tag{3.1}$$

where $k_{ij} = r_{ij}/8$ is the permeability of a straight cylindrical tube, $A_{ij} = \pi r_{ij}^2$ is its cross-section, and $\mu_{\text{eff}} = \mu_2 S_{ij} + \mu_1\left(1 - S_{ij}\right)$ is the volume weighted viscosity due to the two fluids. The pressure difference between node i and j is $p_{ij} = p_j - p_i$, and p_c is now the net capillary pressure difference due to all menisci present in the tube.

The walls of a real porous medium will in general have pores and throats of non-trivial shapes, and of various sizes. This means that the capillary pressure will depend on the position of the menisci. The capillary pressure will be higher at narrower parts of the porous materials, e.g. throats, and smaller at wider parts, e.g. pores. This is incorporated in the model by *choosing* a position dependent capillary pressure. We have choosen an hourglass shape such that there is a maximum capillary pressure in the middle and zero capillary pressure ends of the tube. The radius of the cylindrical tube does therefore represent an effective radius as an approximation to an irregular shaped tube. The capillary pressure due to a meniscus is given by

$$p_c(x) = \pm\frac{2\gamma}{r}\left(1 - \cos\frac{2\pi x}{L}\right), \tag{3.2}$$

where the sign depends on whether a meniscus is advancing or receding. During drainage, the pressure difference across the link must exceed the capillary threshold

in the middle given by $p_t = 4\gamma/R$ for an advancing meniscus to pass through. By this choice we can also have bubbles move both forwards and backwards through a tube.

3.1.4. Fluid Dynamics at the Nodes

Because both the pore and throat volume is represented in the volume of the grid links we have to neglect any actual dynamics at the intersection between links at the nodes themselves. We therefore need to construct rules to approximate the distribution of fluids between links through the nodes. This is a complicated process which we don't have an accurate model of.

The amount of fluid flowing out of each link is accumulated into its neighboring node during a time step. The fluid that has flowed into the node are distributed into neighboring links according to the instantaneous flow rate through those links in such a way that the flow rate and total saturation is preserved. Another important question is if whether the non-wetting or the wetting fluid enters a given link first when both fluids has flowed into the node. We insert the non-wetting fluid first instead of the wetting fluid randomly, but so that the probability is 50% to insert either first.

The rules for distributing the fluids into neighboring links creates an unrealistic large amount of smaller bubbles. These small bubbles will not feel very much resistance from the capillary pressure at all. In a real porous medium there will be larger bubbles present whose size will be restricted by the flow conditions in the pores and throats, the surface tension and the contact angle. We choose the maximum number of bubbles to not exceed 3. If the total number of bubbles in a link exceeds 3, or if the distance between the bubbles are too small, the two nearest bubbles will be merged. Bubbles are merged in such a way that the center of mass is conserved. This will result in unphysical jumps in the capillary pressure, which will show up as pertubations in the total pressure. This will not pose a problem as long as the pertubations are small. The end result is the appearance of larger bubbles.

3.1.5. Units and Dimensional Analysis

Lengths are measured in millimeters, time in seconds, pressure in dyne per millimeter squared, viscosity in 100 Poise, surface tension in dyne per millimeter, and flow rates in millimeter cubed per second.

The capillary number, describing the ratio of viscous to capillary forces, and is given by

$$Ca = \frac{\mu Q}{\gamma \Sigma}, \tag{3.3}$$

where Q is the total flow rate through a horizontal cross-section of the network of area Σ, e.g. the sum of the flow rates through each link along this cross-section. Q/Σ is then the average velocity of both fluids in the network. The viscosity in

(3.3) is the dominant viscosity of the two fluids. The capillary number is constant if the total flow rate is kept constant, but will not be constant if the pressure difference is kept constant.

3.2. Solving the Flow Field and evolving the system

3.2.1. Conservation of Volumetric Flow Rate at the Nodes - The Kirchoff Equations

Conservation of flow rate is forced at the nodes by requiring that the flow rate going into a node is equal to the flow rate going out of the node.

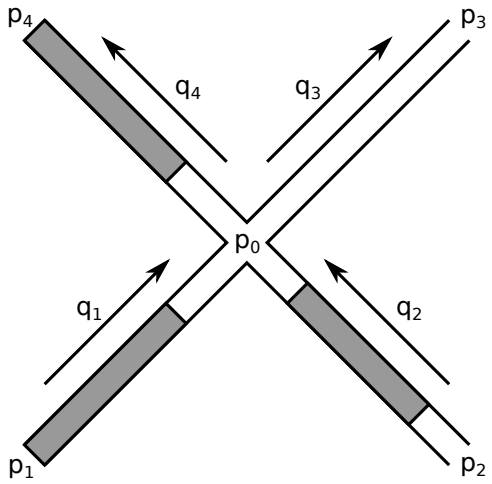

Figure 3.2.: Flow rates and pressure at a node. The arrows depict the positive flow direction.

With respect to figure 3.2, we have

$$q_1 + q_2 = q_3 + q_4. \tag{3.4}$$

Inserting (3.1) and eliminating common terms (π and L) gives

$$\frac{r_1^4}{\mu_1}\left(\Delta p_1 - p_{c,1}\right) + \frac{r_2^4}{\mu_2}\left(\Delta p_2 - p_{c,2}\right) = \frac{r_3^4}{\mu_3}\left(\Delta p_3 - p_{c,3}\right) + \frac{r_4^4}{\mu_4}\left(\Delta p_4 - p_{c,4}\right). \tag{3.5}$$

The pressure differences can be written in terms of the node pressures as $\Delta p_{ij} = p_j - p_i - \delta_{ij}\Delta P$. The term δ_{ij} is equal to one for all the links that connects the nodes at the top row to the nodes at the bottom row of the lattice. This implements the global pressure difference driving the system in the vertical direction. Rearranging equation (3.5), putting all the terms containing the pressures p_j on the left hand side, and the rest on the right had side, gives the matrix equation for the pressure

$$\sum_j A_{i,j} p_j = b_i. \tag{3.6}$$

This is a block tridiagonal matrix equation[1] for the pressure, where the matrix elements $A_{i,j}$ depend on the link radii and effective viscosity only. The right hand side vector elements depend on both the link radii, the effective viscosity, capillary pressures, and the global pressure difference. This matrix in equation (3.6) is symmetric and positive definite, and can be solved efficiently by an iterative matrix solver such as the Conjugate Gradient method.[2] The Conjugate Gradient algorithm is described in detail in [17].

3.2.2. Initial and Boundary Conditions

Two different initial conditions and boundary conditions have been applied, these will be refered to as *single interface* and double interface (or *band*) boundary conditions. The boundaries at the sides of the system will be open with respect to fluid flow, as if they are connected to a reservoir of either non-wetting or wetting fluid, while the boundaries on the top and bottom will be periodic. All boundaries are periodic with respect to pressure. The open boundaries are implemented by removing the fluid in all the links along the boundaries each time step, and replacing it with the fluid of its respective reservoir, effectively transporting fluids that has reached the boundary out of the system.

The network will be filled by both a non-wetting and a wetting fluid. There will initially be a well defined boundary separating both the fluids, either vertical, or a slightly distorted sinusoidal shape to reduce high capillary pressures due to the sharp initial interface. This initial boundary will be refered to as *the non-wetting front*.

The *single interface* boundary condition has one side connected to a non-wetting reservoir, and the other to a wetting reservoir. The system is initialized by filling links with non-wetting fluid sequentually, starting from the boundary connected to the non-wetting reservoir, increasing towards the other boundary until a given non-wetting saturation has been reached. The total saturation is defined as sum of all the volume filled by non-wetting liquid to the volume of the whole network.

The *double interface* boundary condition will be a system where both sides are connected to a reservoir of the same fluid. If the reservoirs contain non-wetting fluids, there will be be a band of wetting fluid in the middle of the system surrounded by wetting fluid. On the other hand, if the reservoirs contain wetting fluid, there will be a band of non-wetting fluid surrounded by wetting fluid. The system is initially filled by first filling the links in the middle of the system, and sequentially moving towards the reservoirs on both sides until a set saturation has been reached.

[1] The matrix in (3.6) is a cyclic block tridiagonal matrix, where the blocks themselves are also cyclic. This is because of the bi-periodic pressure boundary conditions.

[2] The matrix is identical to what one gets by numerically differentiating the two-dimensional Poisson equation with non-constant coefficients using a first order finite difference scheme. That is, the matrix equation resulting from differentiating $\nabla \cdot \big(A(x,y)\nabla P(x,y)\big) = b(x,y)$ numerically. Any algorithm that is used to accelerate these kinds of equation can also be used here.

3.2.3. Solving for a Constant Total Flow Rate

The total volumetric flow rate is defined as the sum of the flow rates through all the links

$$Q = -\sum_{ij} \frac{k_{ij} A_{ij}}{\mu_i j L_{ij}} \left(\Delta p_{ij} - p_{c,ij} \right). \tag{3.7}$$

The total flow rate can be written as a linear function of the global pressure difference [13]

$$Q = A\Delta P + B, \tag{3.8}$$

where the first term depends on the permeability, the effective viscosities of the links and the pressure differences across the links. The second term has contributions from the capillary pressures in addition to the permeability, the effective viscosities of the links and the pressure differences across the links. We can keep the total flow rate constant by finding both the constants A and B and from this find the pressure difference that gives the required flow rate as follows:

First, we solve the pressure equations (3.6) twice for two arbitrary pressure differences, $\Delta P^{'}$ and $\Delta P^{''}$, and calculate the corresponding total flow rate, $Q^{'}$ and $Q^{''}$, we get

$$Q^{'} = A\Delta P^{'} + B, \tag{3.9}$$

$$Q^{''} = A\Delta P^{''} + B. \tag{3.10}$$

From this, we can calculate A and B as

$$A = \frac{Q^{''} - Q^{'}}{\Delta P'' - \Delta P'}, \tag{3.11}$$

$$B = Q^{'} - A\Delta P^{'}, \tag{3.12}$$

which give the global pressure difference

$$\Delta P = \frac{Q}{A} - \frac{B}{A}, \tag{3.13}$$

where Q is now the flow rate calculated from equation (3.3) by specifying a capillary number, $Q = \mathrm{Ca}\gamma\Sigma/\mu$. The flow rate through a given link can be written as a function of the global pressure difference as

$$q = a\Delta P + b. \tag{3.14}$$

Applying the same procedure as for the total flow rate for each link, gives

$$a = \frac{q^{''} - q^{'}}{\Delta P'' - \Delta P'}, \tag{3.15}$$

$$b = q^{'} - a\Delta P^{'}, \tag{3.16}$$

which gives the flow rate through each link for the pressure difference calculated from equation (3.13).

Transverse Flow Rate

The positive direction of the flow is defined in the upward direction, e.g. all the links across a horizontal cross-section will contribute to the total flow rate in the same way, by addition. We can define the flow rate through any cross-section. If the cross-section is horizontal, then the total flow through this plane will be the same for any horizontal plane due to conservation of flow rate at the nodes. The same holds for a vertical plane, the flow through any vertical plane will be the same for any vertical cross-section of the network. By choosing a vertical cross-section, we calculate how much fluid is flowing out of (and into) the system at each open boundary, we will call this the *transverse flow rate*.

To calculate the transverse flow rate requires us to replace the sum over all the local flow rates to a staggered sum due to the rotated grid. Half the links are rotated 45° clockwise and point diagonally in the same direction as the normal vector to the vertical plane, and half the links will be rotated counter-clockwise with respect the y-axis, pointing in diagonally in the opposite direction. This means that the dot-product of the flow-vector through a link and the normal vector to the vertical plane changes sign for every other link for each row. We can calculate the transverse flow rate $Q_\perp$ as

$$Q_\perp = -\left[\sum_r \frac{k_r A_r}{\mu_r L_r}\left(\Delta p_r - p_r^c\right) - \sum_l \frac{k_l A_l}{\mu_l L_l}\left(\Delta p_l - p_l^c\right)\right] = A_\perp \Delta P + B_\perp, \quad (3.17)$$

where r is the set of all links for which $x+y$ is an even integer, and l is the set of all links for which $x+y$ is an odd integer. x and y are the link's x and y coordinates on the lattice, starting from the lower left corner of the lattice.

It is possible to calculate the global pressure difference such that the transverse flow rate remains constant in the same way as it was done when the total flow rate was kept constant. The only difference is to replace Q by $Q_\perp$, A by $A_\perp$ and B by $B_\perp$.

3.2.4. Evolving the System

After having solved the pressure at the nodes, and the local flow rates has been calculated using equation (3.1), we update the position of all the menisci in each link according to the velocity of the fluid flowing through it, as calculated by (2.17). A simple first order Runge-Kutta is used, moving each meniscus in link ij by an amount $\Delta x_{ij} = u_{ij}\Delta t$, where the time step Δt is chosen in such a way that

$$\max_{ij} \Delta x_{ij} < 0.1L. \quad (3.18)$$

A value of 0.1 is found to be sufficient [13] to ensure stability. Any fluid that has been moved out of a link and into a neighboring node are distributed into neighboring links as described in Section 3.1.4. If the number of bubbles in a link after this step exceeds 3, the two nearest bubbles in the link are merged into a single bubble as explained in Section 3.1.5.

4. Results and Discussion

The following parameters have been used in all simulations unless stated otherwise:

- Equal viscosity: $\mu_{nw} = \mu_w = 1$ Poise.
- Surface tension: $\gamma \cos\theta = 3\ \frac{\text{dyne}}{\text{mm}}$.
- Constant link length: $L = 1$ mm.
- Disordered link radius: $r \in [0.1\text{ mm}, 0.4\text{ mm}]$

These are in principle arbitrary except for the range of link radii. The only important quantity is the capillary number, in the sense that a change in either viscosity, length or surface tension scale would be balanced by a change in the flow rate such that the capillary number remains constant. The driving force ΔP only appears on the right hand side of equation (3.6), but implicitly determines the total flow rate and capillary number through equation (3.8).

There are two relevant capillary numbers, one for the flow rate across a horizontal cross-section (the total flow rate), and for the transverse flow rate across a vertical cross-section. As the constant B and $B_\perp$ in equation (3.8) changes with time (but for a constant ΔP), so will the capillary number, and total and transverse flow rate.

We will focus on single interface boundaries instead of double interfaces. By understanding how this displacement process works we can get a better understanding of how it works for a double interface.

4.1. Bubble Stability

The pressure inside of a curved surface will be higher than outside due to surface tension. The capillary pressure will therefore reduce or increase the pressure difference across the tube required to keep the flow rate the same as without a meniscus present (dashed line), depending on whether the meniscus is receding or advancing, as sketched in Figure 4.1. An advancing meniscus during drainage will require a higher pressure difference, and therefore inhibits the flow, representing a barrier for the meniscus to pass through. A receding meniscus on the other hand, as is the case during imbibition, will provide suction and lowers the required pressure difference to reach a certain flow rate.

From this, it follows that a) a non-wetting fluid tend to stay close to the nodes (unless the pressure difference is large enough to overcome the capillary barrier),

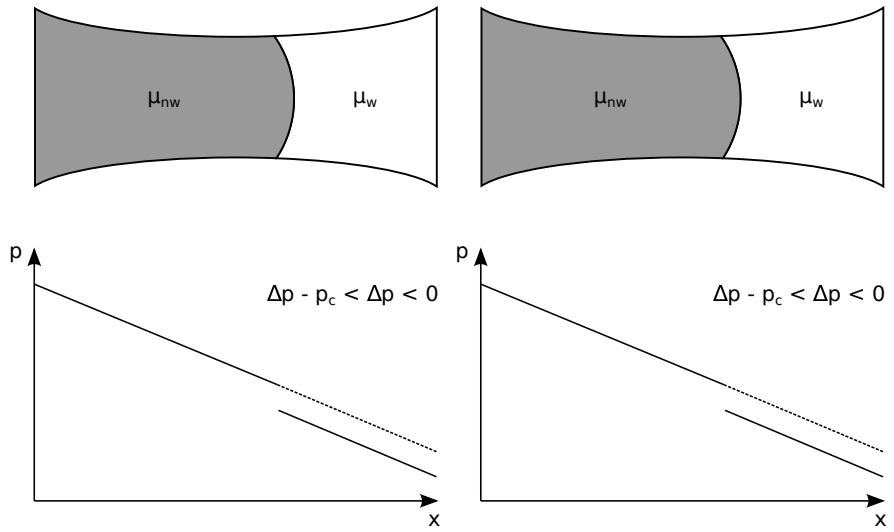

(a) (b)

Figure 4.1.: **(a)**: A single advancing meniscus inside a tube and the corresponding pressure jumps across the meniscus. The appearance of an advancing meniscus increase the pressure difference across the link required to keep up a specific flow rate (as opposed to the dashed line without a meniscus). **(b)**: A single receding meniscus inside a tube and the corresponding pressure jump. The required pressure difference to keep the flow rate with a meniscus the same as that without a meniscus is decreased.

and b) a non-wetting fluid will prefer to invade the widest links (a larger radius means a smaller capillary pressure), while the wetting fluid will invade the narrowest links first and stay away from the nodes. This is the mechanism that tend to stabilize imbibition processes, and destabilize drainage processes.

If the pressure difference across a link is not large enough to overcome the capillary pressure during drainage, the meniscus will not be able to pass through the link.

4.2. Single Interface

4.2.1. Constant Pressure Difference

There are four main regions of interest for the case of a single interface separating the non-wetting and wetting fluid, as illustrated in Figure 4.2. Region 1 and 4 behaves as a single phase, with no menisci present. Region 3 will have wetting fluid flowing through a network with an effective permeability due to the immobile

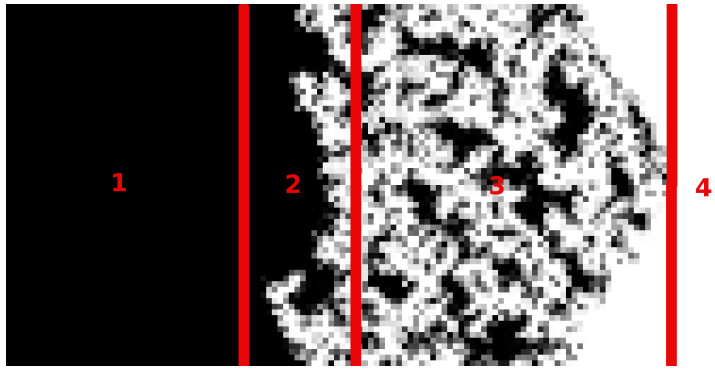

Figure 4.2.: The 4 distinct regions during a simulation. Region 1 contains only non-wetting fluids, flowing as a single phase. Region 2 contains non-wetting front moving towards the non-wetting reservoir. Region 3 contains immobile clusters of non-wetting fluid left behind by the moving non-wetting front, with wetting fluid flowing inbetween the clusters. Region 4 contains only wetting fluids, flowing as a single phase.

non-wetting clusters left behind by the displaced non-wetting front. Region 2 contains the moving non-wetting front, which is displaced by the wetting liquid flowing through region 3. The fluids flows from the bottom to the top, driven by a global pressure difference between the lower and upper row of nodes (with the higher pressure at the bottom row).

If the pressure differences across the links along the initial non-wetting front are not sufficiently large to overcome the capillary thresholds during drainage, then imbibition will dominate. The non-wetting front is displaced by wetting fingers moving in the direction of the average flow direction and towards the non-wetting reservoir, isolating clusters of non-wetting fluid along the way. The non-wetting clusters tend to consist of larger links of non-wetting fluid surrounded by smaller links containing wetting fluids.

When the global pressure difference is small, all non-wetting clusters will remain immobile. Larger pressure differences will result in the creation of smaller cluster. If the pressure difference is large enough such that the capillary barriers holding back a cluster is overcome, it will start moving. At sufficiently higher global pressure differences, all clusters will be mobilized, resulting in a current of non-wetting bubbles moving away from the non-wetting front towards the wetting reservoir.

Figure 4.3 shows three snapshots from a simulation using a global pressure difference of $\Delta P/N_y = 0.5$. The non-wetting liquid is displaced by the wetting fingers along the non-wetting front, leaving behind immobile clusters of non-wetting fluid surrounded by wetting fluid flowing from the wetting reservoir towards the non-wetting front. A limited number of paths of $q \neq 0$ connecting the wetting reservoir to the non-wetting front are present. By comparing the saturation and local flow rates of the links at successive times we can see that the non-wetting fluid is dis-

placed only at the end of these paths.

The total saturation and transverse flow rate as a function of time is shown in Figure 4.4. The saturation will change at a rate proportional to the transverse flow rate, as the non-wetting fluid can only flow out of the network through the non-wetting reservoir. From the figure we can see that the transverse flow rate eventually start fluctuating about a constant negative value, resulting in a constant decrease in saturation. This means that the non-wetting front moves with a constant average velocity towards the non-wetting fluid. The front will move until it has reached the non-wetting reservoir, at which point the simulation is terminated.

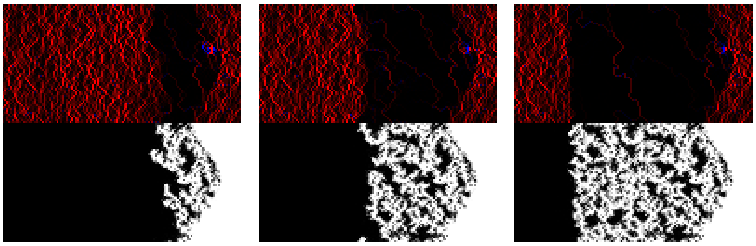

(a) 1000 s (b) 3500 s (c) 8000 s

Figure 4.3.: Flow field (top) and saturation plot (bottom) of three different snapshots of a single interface simulation for a system of $128x64$ links, an initial saturation of 85%, global pressure difference $\frac{\Delta P}{N_y} = 0.5$ at successive times. A red hue (upper plot) represent a positive (upwards) flow rate, while a blue hue a negative flow rate. The saturation plot shows link saturation in grayscale.

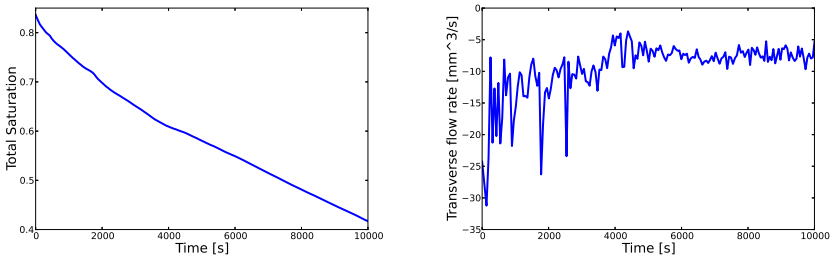

(a) (b)

Figure 4.4.: **(a)** Total saturation as a function of time for the system in Figure 4.3, and **(b)** transverse flow rate as a function of time.

Similarly, Figure 4.5 shows snapshots from the same network as in Figure 4.3, but global pressure difference 8 times larger. The driving force is now large enough to

mobilize some of the non-wetting clusters left behind by the displaced non-wetting front. These clusters break up into bubbles that move from their initial position. The system initially evolves similar to Figure 4.3, but after some time bubbles are moved such that they disconnect the connected paths of wetting fluid displacing the non-wetting front. If no such paths of wetting fluid connecting the wetting reservoir to the front are available, the front will be unable to be displaced and will stop moving. The transverse flow rate will go to zero, as there are no paths for the wetting liquid to flow. This happens in Figure 4.5c. The total saturation and transverse flow rate as a function of simulated time is shown in Figure 4.6. The saturation eventually goes to a constant value, while the transverse flow rate goes to zero as the front stops moving.

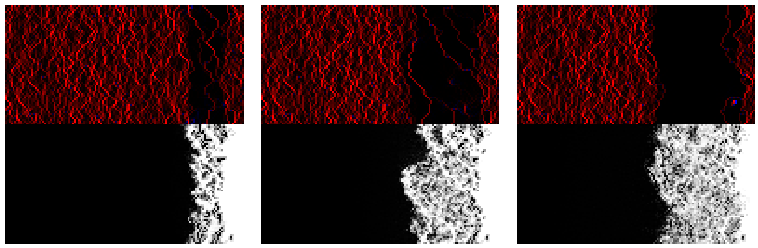

(a) 45 s (b) 175 s (c) 540 s

Figure 4.5.: Plot of the flow field (top) and saturation (bottom) at three different times during a single interface simulation for a system of 128×64 links, an initial saturation of 85%, and global pressure difference of $\frac{\Delta P}{N_y} = 4$ is used.

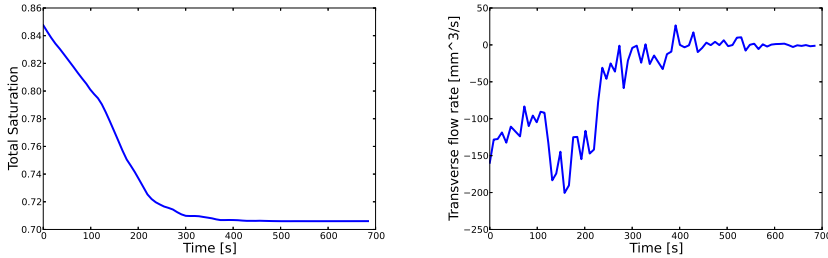

(a) (b)

Figure 4.6.: **(a)** Total saturation as a function of time for the system in Figure 4.5. **(b)** Transverse flow rate as a function of time for the system in Figure 4.5

Finally, Figure 4.7 shows the result of four different simulations at even higher pressure differences. Another network realization is included in addition to the one

already shown in Figure 4.3 and 4.5. In addition simulations where the boundaries have been switched is included. The plots shows a new flow regime appearing at higher pressure differences which depends on the network geometry and boundary conditions. The pressure difference is so large that almost all the clusters left behind imbibition at moving non-wetting front will be mobilized, and a current of non-wetting bubbles flows into the wetting region.

The direction of the transverse flow rate depends on the network realization itself in addition to local behavior at the front. If the non-wetting reservoir is at the opposite side of the network as the direction of the transverse flow rate, as is the case in Figure 4.7b and 4.7c, the total saturation will increase. The non-wetting front becomes unstable, and non-wetting fingers will grow towards the wetting reservoir. These fingers will be broken up into bubbles if the global pressure difference sufficiently large. If the net transverse flow rate is in the same direction of the non-wetting reservoir the non-wetting front will remain stable, and move towards the non-wetting reservoir while non-wetting bubbles broken off from the front will diffuse out to the wetting reservoir.

Figure 4.8 shows the total saturation and transverse flow rate as a function of time for the simulations in Figure 4.7.

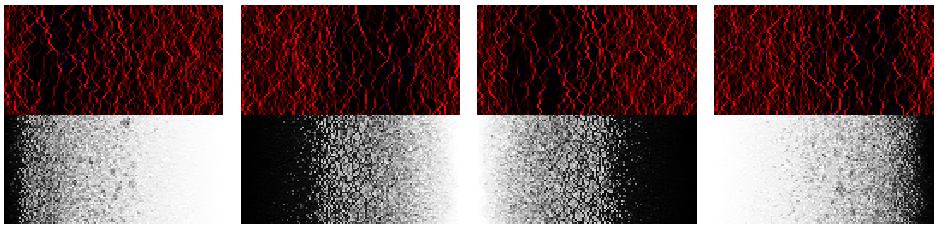

(a) #1, $Q_\perp < 0$ (b) #2, $Q_\perp > 0$ (c) #1, $Q_\perp < 0$ (d) #2, $Q_\perp > 0$

Figure 4.7.: Snapshots of a single interface simulation for two systems (#1 and #2) of 128×64 links, an initial saturation 85%, a global pressure difference $\frac{\Delta P}{N_y} = 16$, recorded after 300 seconds. **(a)** and **(c)** have the same network as in Figure 4.3 and 4.5, while **(b)** and **(d)** have a different network realization. The transverse flow depend only on the network realization, and not on the boundary condition.

4.2.2. Relation to the Transverse Flow Rate

The results in the previous results can be explained as follows: The transverse flow rate is calculated as

$$Q_\perp = -\left[\sum_r \frac{k_r A_r}{\mu_r L_r}\left(\Delta p_r - p_{c,r}\right) - \sum_l \frac{k_l A_l}{\mu_l L_l}\left(\Delta p_l - p_{c,l}\right)\right]. \tag{4.1}$$

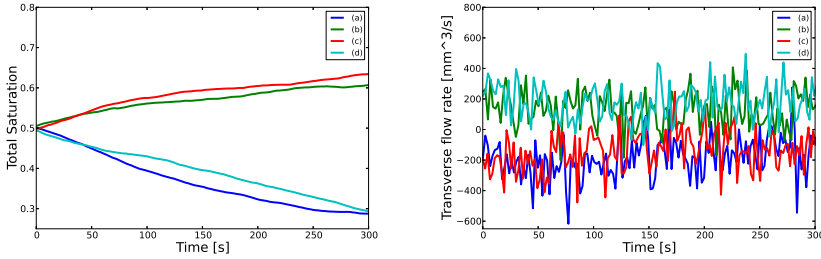

(a) (b)

Figure 4.8.: **(a)** Saturation as a function of time for the system in Figure 4.7. **(b)** Transverse flow rate as a function of time for the system in Figure 4.7

We can separate the effects of the capillary pressure

$$Q_\perp = -\left[\sum_r \frac{k_r A_r}{\mu_r L_r}\Delta p_r - \sum_l \frac{k_l A_l}{\mu_l L_l}\Delta p_l\right] + \left[\sum_r \frac{k_r A_r}{\mu_r L_r} p_{c,r} - \sum_l \frac{k_l A_l}{\mu_l L_l} p_{c,l}\right]. \quad (4.2)$$

We want to write the transverse flow rate as a linear function in the pressure difference, $Q_\perp = A_\perp \Delta P + B_\perp$. The coefficients $A_\perp$ and $B_\perp$ are then calculated as follows: For every snapshot the current bubble configuration is stored, and equation (3.6) is solved multiple times for different values of ΔP, after which a linear fit of $Q_\perp$ as a function of ΔP is performed [1]. $A_\perp$ will only depend on the permeability of the network, while $B_\perp$ will depend on the permeability, the pressure difference across the links, and on the capillary pressure due to menisci present in the network.

Figure 4.10 shows $A_\perp$ as a function of time for the simulations in Figure 4.7a (red) and 4.7b. $A_\perp$ clearly does not change with time, and only depend on the network realization. We can see from the plot that Figure 4.7a (blue line) has $A_\perp > 0$, while Figure 4.7b (red line) has $A_\perp < 0$. This comes from the skewness in the permeability for a finite system due to the disorder of the link radii. $A_\perp$ will dominate over $B_\perp$ for large ΔP. If $A_\perp$ is found once for a given network, we can calculate $B_\perp = Q_\perp - A_\perp \Delta P$ for any time step. If a larger system is used, the number of terms in equation (4.2) will increase, and the value of $A_\perp$ will go to zero as the skewness in the permeability disappears.

If $A_\perp > 0$, we can predict that the transverse flow rate will be positive for large $\Delta P > 0$ (and negative for large $\Delta P < 0$). For small values of ΔP we will find that $B_\perp$ dominates the flow, e.g. imbibition dominates.

When $Q_\perp > 0$, and the non-wetting reservoir is on the left side of the system and vice versa, as is the case in Figure 4.7b and 4.7c, we can expect the front to stop moving, and drainage will dominate along the non-wetting front. If the opposite holds imbibition will dominate, as is the case in Figure 4.7a and 4.7d.

[1] Only two different ΔP are needed, as the $Q_\perp$ is a linear function in ΔP.

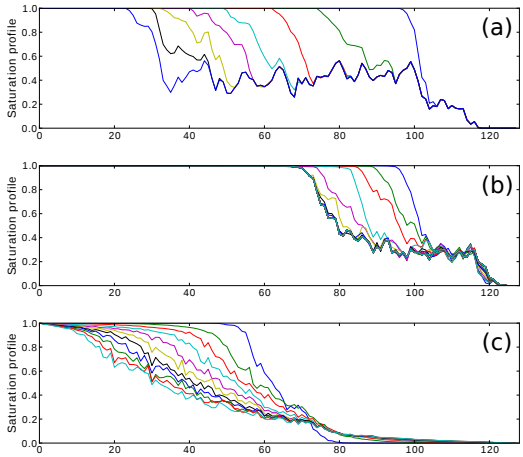

Figure 4.9.: Saturation profile at constant time intervals for a single interface system corresponding to **(a)**: Figure 4.3 (100000 time step intervals) **(b)**: Figure 4.5 (5000 time step intervals), and **(c)**: Figure 4.7a (10000 time step intervals). **(a)** and **(b)** has an initial saturation of 85%, while **(c)** has an initial saturation of 50%.

4.2.3. Constant Transverse Flow Rate

The global pressure is not a good parameter to characterize the displacement of the non-wetting front, as it does not take into account the disorder of the system. A better characteristic number would be the transverse capillary number analogously to the global capillary number

$$\mathrm{Ca}_\perp = \mu Q_\perp / \gamma \Sigma_\perp. \tag{4.3}$$

where $\Sigma_\perp$ is area of a vertical cross-section of the system and $Q_\perp$ is the transverse flow rate through it. We can get more insight into the displacement process along the non-wetting front by forcing this transverse capillary number to remains constant during a simulation by adjusting the global pressure difference.

Figure 4.11 and 4.12 show the evolution of a wetting finger displacing the non-wetting front for transverse capillary numbers $\mathrm{Ca}_\perp = -10^{-5}$ and $\mathrm{Ca}_\perp = -5 \times 10^{-5}$ (the sign is to ensure that the direction of the transverse flow is in the direction of the non-wetting reservoir), with a 10000 time step interval between each snapshot. The smallest $\mathrm{Ca}_\perp$ shows a single thin wetting finger displacing the non-wetting front at only one location, and approximately in the same direction. The larger $\mathrm{Ca}_\perp$ shows a more irregular displacement of the front, with the front being displaced at several locations and directions, leaving behind smaller clusters than that for the smaller $\mathrm{Ca}_\perp$. The transverse capillary number are in general a couple orders of magnitude smaller than the global capillary number.

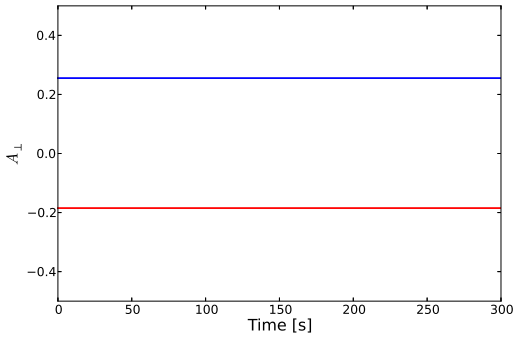

Figure 4.10.: $A_\perp$ as a function of time during the simulation of a 128×64 system at $\Delta P/N_y = 16$, corresponding to Figure 4.7a (red) and 4.7b (blue)

When keeping the capillary number constant the pressure is adjusted accordingly. If there are no paths for the wetting fluid to connect to the non-wetting front the pressure difference will increase until a new path has been created. This means that the global capillary number will increase, and often so much that the clusters in the region behind the non-wetting front temporarily mobilize. This method is therefore not suitible for analyzing the behavior away from the front.

There is also no control over the sign of the global pressure difference, whose sign might be positive or negative, or it may fluctuate depending on the local distribution of menisci.

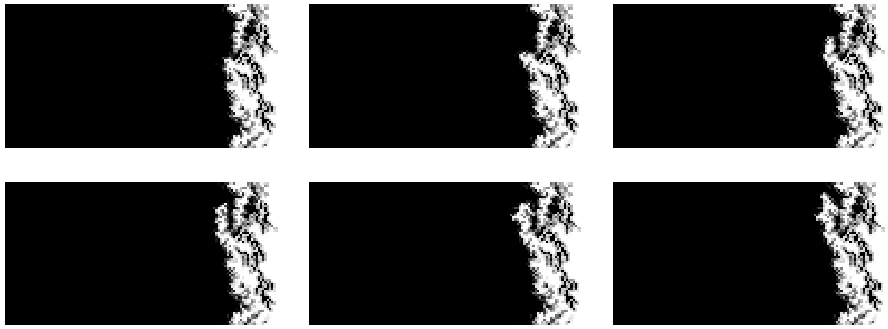

Figure 4.11.: Saturation evolution of a constant transverse flow rate simulation at $\mathrm{Ca}_\perp = -10^{-5}$ in intervals of 10000 time steps. A single wetting finger displace the front in one direction.

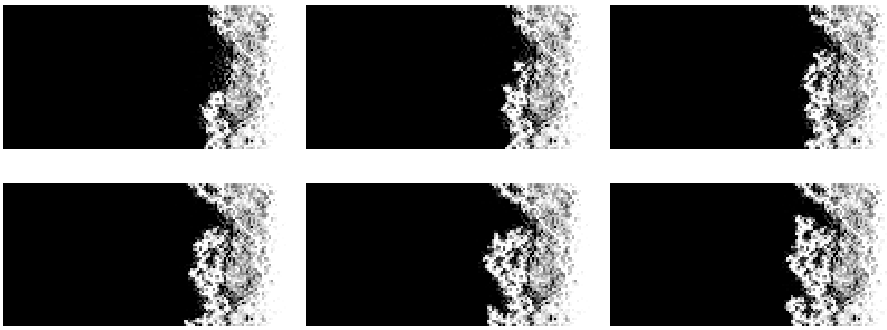

Figure 4.12.: Saturation evolution of a constant transverse flow rate simulation at $\mathrm{Ca}_\perp = -5 \times 10^{-5}$ in intervals of 10000 time steps.

4.3. Double Interface

In the single interface simulation the non-wetting fluid that was displaced along the non-wetting front by the wetting fluid moved out of the system through the non-wetting reservoir. For a band of non-wetting fluid surrounded by wetting fluid there will not be any non-wetting reservoirs for the non-wetting fluid to be transported out of the system. If the global pressure difference is not large enough so that the non-wetting clusters that are created during imbibition along the fronts are unable to move, the front will therefore be stable. By increasing the pressure difference so that most clusters are mobilized, both the fronts may be displaced at the same time. Transport of non-wetting bubbles out of the system by diffusion will be the only way to transport non-wetting out of the system. This is the cause of the instability observed by Ramstad *et al.*

The value of $A_\perp$ will be the same irregardless of the boundary and initial conditions. We can therefore not expect the two fronts to move with the same velocity. We can on the other hand expect that one of the fronts will be dominated by imbibition, while the other by drainage unless $A_\perp \approx 0$. If $A_\perp \approx 0$ we can expect the behavior of the two fronts to be similar. Figure 4.13 shows the saturation profile $S_{nw}(x)$ for three different realizations of 512×32 links, having a positive, negative, and close to zero $A_\perp$, respectively. Figure 4.13a and 4.13b shows one front dominated by drainage and one front dominated by imbibition, with the imbibition front moving with a constant velocity and shape towards the non-wetting fluid. Figure 4.13c is much slower than 4.13a and 4.13b and both fronts move at the same time. It is not clear whether they move with a constant velocity. Only the shape of the upper part saturation profile of Figure 4.13c seems to remain constant, as the tails of the curve tend to smoothen out due to diffusion.

We can also shed some light on the case when a band of wetting fluid is surrounded by non-wetting fluid. The wetting fluid will not be in contact with a wetting reservoir, and imbibition cannot happen along the non-wetting fronts. A diffusive current of non-wetting bubbles will flow through the wetting region until

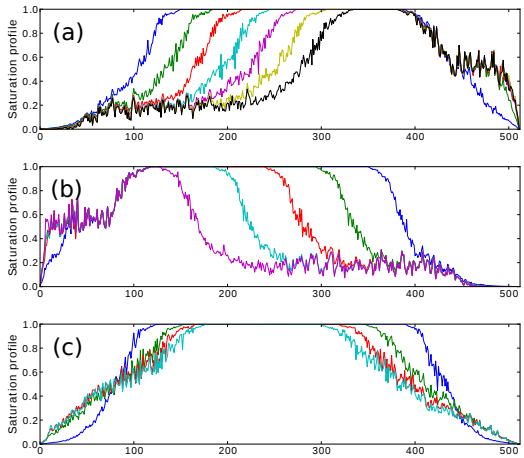

Figure 4.13.: **(a)**: Saturation profile as a funtion of time for a double interface system of size 512×32 links where $A_\perp > 0$ and $\Delta P/N_y = 16$. The curves are 100000 time steps apart. **(b)**: $A_\perp < 0$, and **(c)**: $A_\perp \approx 0$, 200000 time steps apart

the net flow of bubbles is zero, resembling the drainage dominated cases in Figure 4.7.

For a complete comparison to the results presented by Ramstad *et al.* one need to consider the more intricate details of the model. In particular the rules for merging bubbles when the total number of bubbles in a link exceeds a maximum number will have an effect on the displacement of the non-wetting front. The maximum number of bubbles would also effect the diffusive region behind the front. If one allows too many non-wetting bubbles, the diffusive current of bubbles broken off from the non-wetting front will tend to break up into as many bubbles as possible, however small.

5. Conclusion and Outlook

We have been successful in providing an explanation for the displacement processes at the interface separating a non-wetting and a wetting fluid flowing in parallel in a two-dimensional dynamic network simulator. The displacement processes along the non-wetting front has been identified as a competition of imbibition and drainage processes at the pore scale. Whether drainage or imbibition dominate the displacement process depend on the permeability of the network as a whole, the magnitude of the global pressure difference, and on the distribution of the capillary pressures in the system.

We find that when the non-wetting front is displaced by imbibition it moves with a velocity proportional to the transverse flow rate, the flow rate in the direction perpendicular to the driving force. If the transverse flow rate fluctuate about a constant value we find that the front moves with a constant velocity. The front will be displaced along the narrowest links, leaving behind immobile clusters of non-wetting liquid concentrated in larger links with wetting fluid flowing around them.

The displacement at the non-wetting front is characterized by the transverse capillary number in the same way as the global capillary number characterize the displacement front during imbibition and drainage displacements perpendicular to the front separating the fluids. The transverse capillary number depends on the global pressure difference driving the flow in the direction parallel to the front. The shape of the saturation profile $S_{nw}(x)$ will depend on the driving force, with the size of the clusters in the foam layer decreasing as the pressure difference increases.

The instability that appears when a band on non-wetting fluid is surrounded by wetting fluid flowing in parallel above a critical value of the capillary number is explained as the result of the mobilizing of the clusters of non-wetting fluid left behind during imbibition at the fronts separating the non-wetting fluid from the rest of the system. When there are two non-wetting front, and the driving pressure is not large enough to mobilize said clusters, the front will stabilize, and stop moving.

The main goal for future work would be to include the effects of wetting films and snap-off mechanics during imbibition displacements. A dynamic network model including these was developed by Tørå *et al.* [18]. Investigating the case where the viscosity of the two fluids do not match should also be considered. Finding a way to properly model the dynamics of the mixing of fluids at the nodes, the distribution of fluids to neighboring links, and understanding the effect of different rules to merging bubbles should also be highly prioritized.

Bibliography

[1] S. E. Buckley and M. C. Leverett, Transactions of the AIME **146**, 107 (1942).

[2] S. Whitaker, Transp. Por. Media **1**, 3 (1986).

[3] J. Bear, *Dynamics of Fluids in Porous Media* (Dover, New York, 1988).

[4] M. Sahimi, *Flow and Transport in Porous Media and Fractured Rock* (VCH, Weinheim, 1995).

[5] E. W. Washburn, Phys. Rev. **17**, 273 (1921).

[6] E. B. Dussan V. , Annu. Rev. Fluid Mech. **11**, 371 (1979).

[7] R. Lenormand, J. Phys. : Condens. Matter **2**, SA79 (1990).

[8] R. Lenormand, E. Touboul and C. Zarcone, J. Fluid Mech. **189**, 165 (1988).

[9] R. G. Hughes and M. J. Blunt, Transp. Porous Media **40**, 295 (2000).

[10] T. Ramstad, A. Hansen, Phys. Rev. E. **78**, 035302(R)(2008).

[11] L. D. Landau, E. M. Lifshitz, *Fluid Mechanics* Vol. 6 (2nd ed.) (Butterworth-Heinemann/Elsevier, Amsterdam, 1988).

[12] D. Wilkinson and J. F. Willemsen, J. Phys. A: Math. Gen, **16**, 3365 (1983).

[13] E. Aker, K. J. Måløy, A. Hansen, G. G. Batrouni, Transp. Porous Media **32**, 163, (1998).

[14] H. A. Knudsen, E. Aker, A. Hansen, Transp. Porous Media **47**, 99 (2002).

[15] T. Ramstad, A. Hansen, Phys. Rev. E **73**, 026306 (2006).

[16] S. Sinha, M. Grøva, T. B. Ødegården, E. Skjetne, and A. Hansen, Phys. Rev. E **84**, 037303 (2011).

[17] G. G. Batrouni, A. Hansen, Journ. Stat. Phys. **52**, 747 (1988).

[18] G. Tørå, P-E. Øren, A. Hansen, Transp. Porous Media **92**, 145 (2012).

A. Flow Program

The source code for the program used in this thesis can be found with instructions on Github, with a copy of the source code as it was as of the time of writing this manuscript.
`https://github.com/vassvik/parallel-flow-thesis`.